Computational Analysis of Marine-Propeller Performance Using Transition-Sensitive Turbulence Modeling

Xiao Wang
Assistant Research Professor
Center for Advanced Vehicular Systems (CAVS),
Mississippi State University,
Mississippi State, MS 39762
e-mail: xwang@cavs.msstate.edu

Keith Walters
Associate Professor
Department of Mechanical Engineering,
Mississippi State University,
Mississippi State, MS 39762;
Center for Advanced Vehicular Systems (CAVS),
Mississippi State University,
Mississippi State, MS 39762
e-mail: walters@cavs.msstate.edu

Almost all computational fluid dynamics (CFD) simulations of flow around marine propellers use turbulence models that are only well suited for fully turbulent flows, which in some cases may lead to accuracy degradation in the prediction of propeller performance characteristics. The discrepancy between computed thrust and torque and corresponding experimental data increases with increasing propeller load. This is due in part to the fact that a large laminar flow region is found to exist and turbulence transition takes place on propeller blades of model scale and/or under high-load conditions. In these cases, it may be necessary to consider boundary-layer transition to obtain accurate results from CFD simulations. The objective of this work is to perform simulations of a marine propeller using a transition-sensitive turbulence model to better resolve the propeller flow characteristics. Fully turbulent flow simulations are also performed for comparison purposes at various propeller load conditions. Computational results are analyzed and compared with water-tunnel and open-water experimental data. It is found that the applied transition-sensitive turbulence model is better able to resolve blade-surface stresses, flow separations, and tip-vortex originations, and, consequently, improve the prediction accuracy in propeller performance, especially under high-load conditions. Furthermore, solutions obtained using the transition-sensitive turbulence model show tip-vortex flows of higher strength, whereas results by the standard k-ω SST turbulence model indicate excessive dissipation of the vortex core. [DOI: 10.1115/1.4005729]

1 Introduction

Three-dimensional computational fluid dynamics (CFD) simulations employing Reynolds-averaged Navier-Stokes (RANS) turbulence models have made considerable contributions to propeller theory and become useful tools for propeller design and analysis. Among many unresolved issues in RANS calculations of marine-propeller performance, turbulence transition has been recognized as a key factor directly associated with viscous effects of propeller flows, such as boundary-layer development, scale effects, and tip and hub vortices. Nevertheless, few, if any, RANS calculations in the open literature have been performed that consider laminar-to-turbulent transition in marine-propeller simulations. The objective of this study is to perform marine-propeller CFD simulations using both fully turbulent and transition-sensitive eddy-viscosity turbulence models, and to compare the results between the two approaches. Results are also compared to experimental data to determine whether or not boundary-layer transition plays an important role in the calculation of performance characteristics, and to judge the relative predictive capability of the two different models used in the study, for this class of problem.

The marine propeller 5168 (P5168) is a representative propeller geometry with available detailed velocity field laser doppler velocimetry (LDV) measurements and cavitation inception measurements [1]. Data obtained from this model have been used extensively to provide validation for RANS calculations, with specific interest in predicting tip-vortex flow characteristics. Many RANS calculations for the viscous flow around P5168 have been conducted with various codes and turbulence models. The CFDSHIP-IOWA [2] code was used for calculations at near design operating conditions using a blended k-ω/k-ε turbulence model. Rhee and Joshi [3] performed simulations using the commercial code FLUENT using both the k-ω and Reynolds stress transport turbulence models. Hsiao and Chahine [4] used the INS3D code with the Baldwin-Barth one-equation turbulence model to simulate the scaling of tip-vortex cavitation inception. Hsiao and Pauley [5] also used the Baldwin-Barth model and demonstrated that the model produces an overly diffusive and dissipative tip-vortex core. Oh and Kang [6] employed a modified k-ε turbulence model to account for swirling flow and captured the tip-vortex flow more accurately, but the strength of the vortex was still weakly predicted.

In many of these numerical studies, the predictions of the boundary layer on the blade show reasonable agreement with measurements in the turbulent boundary-layer region, but laminar and transitional boundary layers cannot be represented because the flow is assumed to be fully turbulent in the calculation. As a consequence, the accuracy in thrust and torque prediction has been shown to deteriorate with reduced advance ratio [3].

Similar results have been obtained for RANS calculations using other propeller geometries. For example, Stanier [7] performed computations of propeller DTRC4119, C659 and C660, using a 3-D version of the Baldwin-Lomax mixing length model. Chen and Stern [8] similarly performed computations of marine propeller P4318 with the Baldwin-Lomax model. In the work of Funeno [9], the commercial CFD code STAR-CD was used with the RNG k-ε model to study hub vortex and scale effects for a conventional propeller and a highly skewed propeller. Agreement between measured and computed thrust and torque was shown to improve with increasing Reynolds number.

This paper seeks to identify and address at least one potential reason for discrepancy between simulations and experiments. Significantly, all of the RANS calculations mentioned above are based on the assumption that flows are fully turbulent around a

Contributed by the Fluids Engineering Division of ASME for publication in the JOURNAL OF FLUIDS ENGINEERING. Manuscript received December 22, 2010; final manuscript received December 2, 2011; published online July 20, 2012. Assoc. Editor: Frank C. Visser.

marine propeller regardless of the characteristic Reynolds number. Even though most RANS calculations have achieved reasonable agreement in the prediction of overall propeller performance and local flow characteristics at near design conditions, a few common issues still remain to be resolved. These include excessive vortex diffusion and dissipation, and decreasing accuracy in predicted thrust and torque with increased propeller load, as compared with model scale experiments.

With regard to the latter point, it has in fact been well recognized that turbulence models play an important role in propeller flow simulations. Experiments have shown that laminar flow exists over a large area of the propeller blade surface in model scale test cases, up to 60% of the radial span, and that turbulence transition occurs on blade surfaces [9]. Rhee and Joshi [3] demonstrated improvement in CFD predictions by running fully laminar simulations, and concluded that a model capable of predicting both laminar and turbulent regions would further improve predictive capability. However, fully turbulent flows are usually assumed in marine-propeller CFD computations due primarily to the lack of a general and robust turbulence transition model. The ability to accurately predict transitional fluid flow behavior can potentially have a significant impact, enabling computational tools that more effectively meet the needs of modern propeller design and analysis. To that end, the focus of this paper is to apply a three-equation transition-sensitive k-ω model previously developed and documented by Walters and Cokljat [10] in the computation of marine propeller 5168. Results are evaluated to determine the ability of the model to correctly resolve the flow physics associated with viscous flow effects, and to evaluate the relative importance of boundary-layer transition in the prediction of marine-propeller flows. The RANS solver used in this effort is the Loci/CHEM [11] code, an in-house, unstructured, finite-volume CFD code that has been used previously for a wide variety of aerodynamics simulations [12–14] as well as other application areas [15,16].

In the following, brief descriptions of the transition-sensitive turbulence models and the Loci/CHEM solver system are provided in Sec. 2. The propeller geometry and unstructured mesh generation are detailed in Sec. 3. In depth discussion and analysis of the propeller simulations, flow characteristics, and merits of the transition-sensitive turbulence model are presented in Sec. 4. Summary and concluding remarks are included in Sec. 5.

2 Turbulence Model and Loci/CHEM Flow Solver

A number of methods for incorporating boundary-layer transition into CFD simulations are available, ranging from "engineering insight" to select a predetermined transition location, to Direct Numerical Simulation (DNS) [17] to predict the transition process in its entirety. Within the context of Reynolds-averaged Navier-Stokes (RANS) modeling, recent efforts have led to the development of models specifically designed to predict transitional behavior. This may be accomplished by coupling empirical transition models [18–22] to commonly used eddy-viscosity turbulence models, or through the use of modified versions of the turbulence models that reproduce the transition process. Difficulties in implementing empirical correlations include the fact that most correlations are based on downstream distance (x) or boundary-layer momentum thickness (θ), and the determination of these quantities requires the use of nonlocal or integrated variables in the simulation. The second approach is more general, and typically includes additional transport equations and/or model terms to include the effects of transition on the flow field prediction. Examples include phenomenological models [23–25] and correlation-based models [26–28], and versions of both have recently been released in commercial CFD codes [29]. The most practical of these approaches are single-point models, which do not require nonlocal information to be included in the model terms. These include the phenomenological models of Wang and Perot [24], Walters and Leylek [25], and Walters and Cokljat [10], and the correlation-based model of Menter et al. [28]. Single-point models are generally applicable and are straightforward to implement into existing codes for CFD prediction of laminar, transitional, and turbulent flow. Whereas significant room for improvement remains, all of these models have significantly extended the modeling toolkit available to CFD end users, and allow more physical mechanisms to be investigated in the analysis of complex flow systems.

For this study, a previously documented transition-sensitive turbulence model [10] has been implemented into the Loci-CHEM solver system [11]. The model is a three-equation eddy-viscosity type, with transport equations solved for turbulent kinetic energy (k_T), specific dissipation rate (ω), and laminar kinetic energy (k_L). The laminar kinetic energy concept was first introduced by Mayle and Schulz [30], and is used to represent the energy of velocity fluctuation modes that arise in the boundary layer prior to transition, with structural and dynamic characteristics dramatically different from fully turbulent flow. These fluctuations are related; for example, to Tollmein-Schichting waves that are precursors to natural transition, or the Klebanoff modes that characterize bypass transition initiation. In the model, the transition process itself is represented as a transfer of energy from the laminar kinetic energy, k_L, to the turbulent kinetic energy, k_T. A k-ε model based on this approach was originally proposed by Walters and Leylek [25]. The model used here represents the most recent variant of this approach. It has been demonstrated for a number of test cases and is currently available in the Ansys FLUENT commercial flow solver. Details of the model derivation and equations, as well as further validation test case examples, are available in Ref. [10].

An example of the model performance is given in Fig. 1, which shows the predicted skin friction coefficient, C_f, for a flat plate boundary layer with different levels of freestream turbulence. The results shown were obtained as part of the verification and validation tests for implementation of the model into the flow solver Loci-CHEM. The experimental data included in Fig. 1 for comparison are from the T3 cases of the ERCOFTAC database [31].

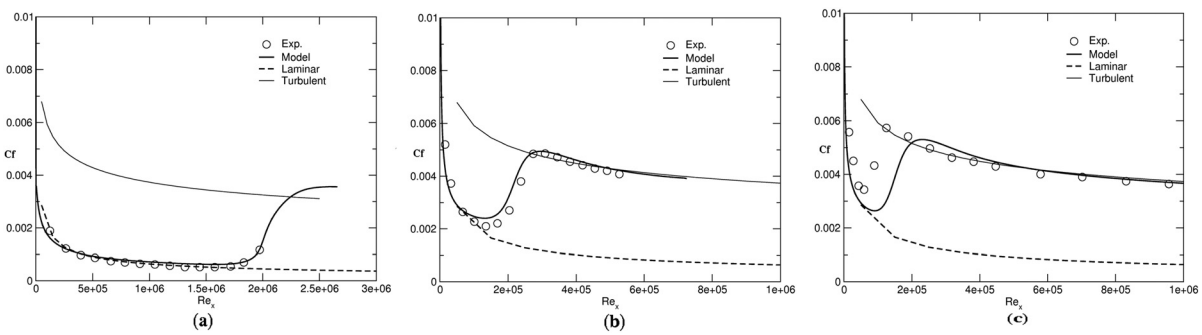

Fig. 1 Prediction of skin friction coefficient for flat plate boundary layer using transition-sensitive k-ω model: (*a*) $Tu_\infty = 0.8\%$, (*b*) $Tu_\infty = 3.3\%$, and (*c*) $Tu_\infty = 6.5\%$

Table 1 Simulation flow conditions

Advance coefficient $J = U_\infty/(nD)$	Free stream velocity U_∞/(m/s)	Rotational speed (rpm)	Reynolds number Re (10^6)	Blade Reynolds number Re_b (10^6)
0.5	4.87	1450	1.95	5.40
0.98	7.893	1200	3.17	4.62
1.1	10.70	1450	4.29	5.65
1.27	11.08	1300	4.44	5.16
1.51	11.73	1150	4.67	4.69
1.6	15.57	1450	6.25	5.99

The Loci-CHEM flow solver system is a fully featured Navier-Stokes solver developed using the Loci [32] framework for non-equilibrium flows including chemical reactions. The solver uses advanced generalized grid algorithms based on cell-centered finite-volume methods and high-resolution Riemann solvers. A preconditioning scheme [33] is available for very low Mach number applications, which can be utilized to solve incompressible flows. Details of the flow solver including physical models and numerical methods are available in Ref. [11].

3 Marine Propeller 5168 and Grid Generation

The marine-propeller geometry studied in this work is the David Taylor Propeller 5168. It is a five-bladed, controllable-pitch propeller with a design advance coefficient of $J = 1.27$. The diameter of the propeller is 0.4027 m. The details of the propeller geometry can be found in Chesnakas and Jessup [1]. 3D LDV velocity measurements were made behind Propeller 5168 in the Carderock Division Naval Surface Warfare Center (CDNSWC) 36-in. water tunnel operating with uniform inflow at four advance coefficients: $J = 0.98$, 1.1, 1.27, and 1.51. Propeller performance, cavitation inception and velocity components with sufficient spatial resolution were measured to reveal the details of the tip-vortex flow. The same propeller has been open-water tested in the CDNSWC towing basin to assess its open-water performance under broader load conditions with advance ratio (J) ranges from 0.0 to 1.60.

In this study CFD simulations using both the transition-sensitive turbulence model [10] and the k-ω SST turbulence model [34], are conducted at six propeller load conditions as summarized in Table 1. The freestream velocities and propeller rotational speeds for cases $J = 0.98$, 1.1, 1.27, and 1.51 are directly based on the water-tunnel test report [1]. In addition, for the open-water test cases, two additional advance coefficients ($J = 0.5$, 1.6) were simulated. Because the propeller rotational speeds (or the freestream velocities) used in the definition of advance ratio J are not specifically delineated, an arbitrary rotational speed of 1450 rpm was selected, and corresponding freestream velocities were estimated based on the definition of J. Both the freestream Reynolds number and the blade Reynolds number are listed in Table 1, indicating the characteristics of inflow and rotating flows.

Body-fitted mixed-element type unstructured grids suitable for viscous simulations were used. Fully unstructured triangular surface grids were generated using SolidMesh [35], the in-house MSU CAVS mesh generation tool. Volume grids were constructed using the Advancing-Front Local Reconnection (AFLR) grid generation technique [36,37]. The outer boundary of the computational domain extended 3.5D in both the upstream and downstream directions and 1.5D in the radial direction. This domain extent is believed to be sufficiently far from the propeller based on existing studies conducted by other researchers [3,4,38], in which similar or smaller domains were adopted.

In transitional flows, the transition process and the location and extent of laminar separation bubbles are expected to be more sensitive to grid resolution than fully turbulent flow features. It is therefore important to ensure sufficient grid refinement in the simulations when turbulence transition is included. A grid resolution study was conducted to provide insight into the impact of grid spacing on performance predictions for the marine propeller. Three grids, referred to as coarse, medium, and fine, were generated based on the same geometry definition. Smaller edge spacings were applied to blade leading edge, trailing edge and tip regions, whereas relative larger spacings were used near mid-chord, root, and shaft regions. During the grid refinements, grid spacing on the propeller surfaces and outer boundaries were scaled by a global factor to achieve distinct resolution levels. However, the grid spacing in the blade edge region is very critical to the resulting mesh quality and often requires additional manual adjustment. It was necessary to further refine the grid spacing at blade edges, especially in regions near the tip, because of the very thin edge of the propeller. Quality of the surface mesh in this sensitive region also affects the quality of volume grid in its vicinity. A maximum cell-to-cell volume ratio less than 20 was achieved in all three grids. The total number of cells in the coarse, medium, and fine grids was 4.09×10^6, 11.46×10^6, and 22.43×10^6, respectively. The normal spacing of the first grid point off the propeller surface was within a dimensionless distance of $y^+ < 0.5$ over all the propeller surfaces to ensure proper viscous sublayer resolution. Prism cells were generated in the viscous layer near the surface to a distance based on an estimated boundary-layer thickness of approximately 10^{-3}R. The normal spacing increased geometrically and the maximum allowable value of the normal spacing growth rate was 1.5. Cells of tetrahedral, prism, and pyramid topology were generated to fill the remainder of the domain to the outer boundary surface. Illustrations of grid boundary layer and field resolution are shown in Fig. 2. In the grid resolution study, only case $J = 1.1$ was simulated on each grid with both shear stress transport (SST) model and the transition-sensitive model (TSM). Detailed grid parameters are summarized in Table 2, along with the comparison of predicted thrust and torque coefficients computed on each grid using the k-ω SST, and TSM models.

For both the k-ω SST, and TSM turbulence models, the integrated thrust and torque varied as the grids were refined. Large differences are shown between the coarse and medium refinement grids, but little change was found between the medium and fine resolution grids (max. 3%). Aside from the overall thrust and

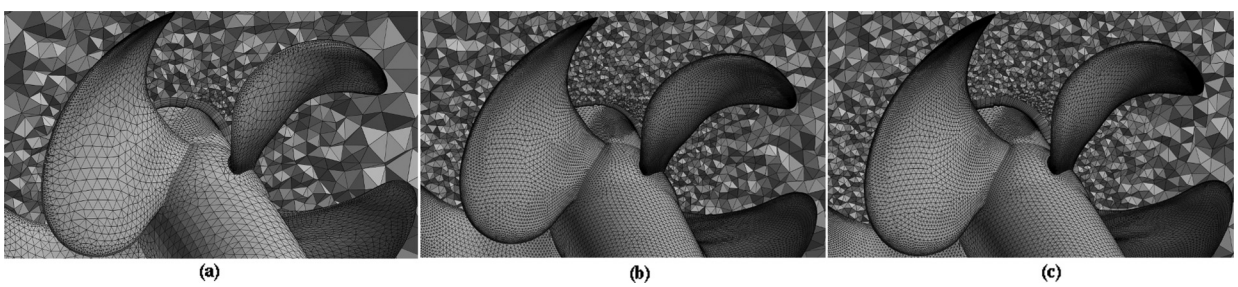

Fig. 2 Surface mesh and cutting plane through volume mesh: (*a*) coarse, 4.09M cells, (*b*) medium, 11.46M cells, and (*c*) fine, 22.43M cells

Table 2 Grid parameters, propeller performance for grid resolution study

			Thrust coefficient k_T (Exp. 0.307)		Torque coefficient k_Q (Exp. 0.078)	
Mesh	Volume grid	Surface grid	SST	TSM	SST	TSM
Fine	22.43 M cells 8.15 M nodes	170 K points 341 K triangles	0.263	0.282	0.089	0.081
Medium	11.46 M cells 3.69 M nodes	100 K points 202 K triangles	0.269	0.291	0.090	0.080
Coarse	4.09 M cells 1.48 M nodes	43 K points 86 K triangles	0.232	0.230	0.096	0.083

torque, the circumferential–averaged axial and radial velocities for the grid convergence tests are shown in Fig. 3. The SST model obtained almost identical results on the medium and fine grids suggesting that the medium grid yields results that are nearly grid independent. The TSM model was found to be more sensitive than the SST model to grid refinement level. However, for the fine grid, the grid size is nearly doubled versus the medium grid and the improvement in results is relatively small with limited impact on the prediction of overall force and thrust. Thus the medium refinement grid was deemed sufficient for efficiently predicting the integrated force and moment acting on the propeller, and was used in this work.

4 Test Cases

4.1 Simulation Details. CFD simulations were conducted at the six load conditions summarized in Table 1. For each load condition, two simulations were performed—a fully turbulent simulation using the k-ω SST turbulence model and a transition simulation using the transition-sensitive turbulence model (TSM). The freestream turbulence conditions were not reported explicitly in the experimental study [1]. However a fluctuation RMS velocity of $q = 0.02$, equivalent to $Tu = 2\%$, is shown at a downstream location ($x/R = 0.2386$ in case $J = 1.1$) at 70% span throughout most of the passage. Considering the freestream region should have lower turbulence intensity than the region behind the rotor, constant freestream turbulence intensity $Tu = 1\%$ was chosen for all the computational cases in this work. The freestream turbulent kinetic energy was then determined based on the turbulence intensity assuming isotropic freestream turbulence. In the absence of experimental data for turbulence length scale, a freestream value was chosen such that the ratio of turbulent to molecular viscosity was approximately 10. For the TSM model, k_L was set to zero on farfield boundary surfaces.

In the k-ω SST model, the Menter's [39] wall boundary conditions were used, in which $k_T = 0$, and a finite value of ω is imposed at the wall based on the distance from the first cell center to the solid wall. In the TSM model, the no-slip condition is enforced for k_T and k_L at a solid wall

$$k_T = k_l = 0 \tag{1}$$

and a zero-normal-gradient condition is used for ω:

$$\frac{\partial \omega}{\partial \eta} = 0 \tag{2}$$

where η is the wall-normal coordinate direction. Note that the wall boundary condition of ω (Eq. (2)) is substantially different from that used in the k-ω SST model. This is because of the

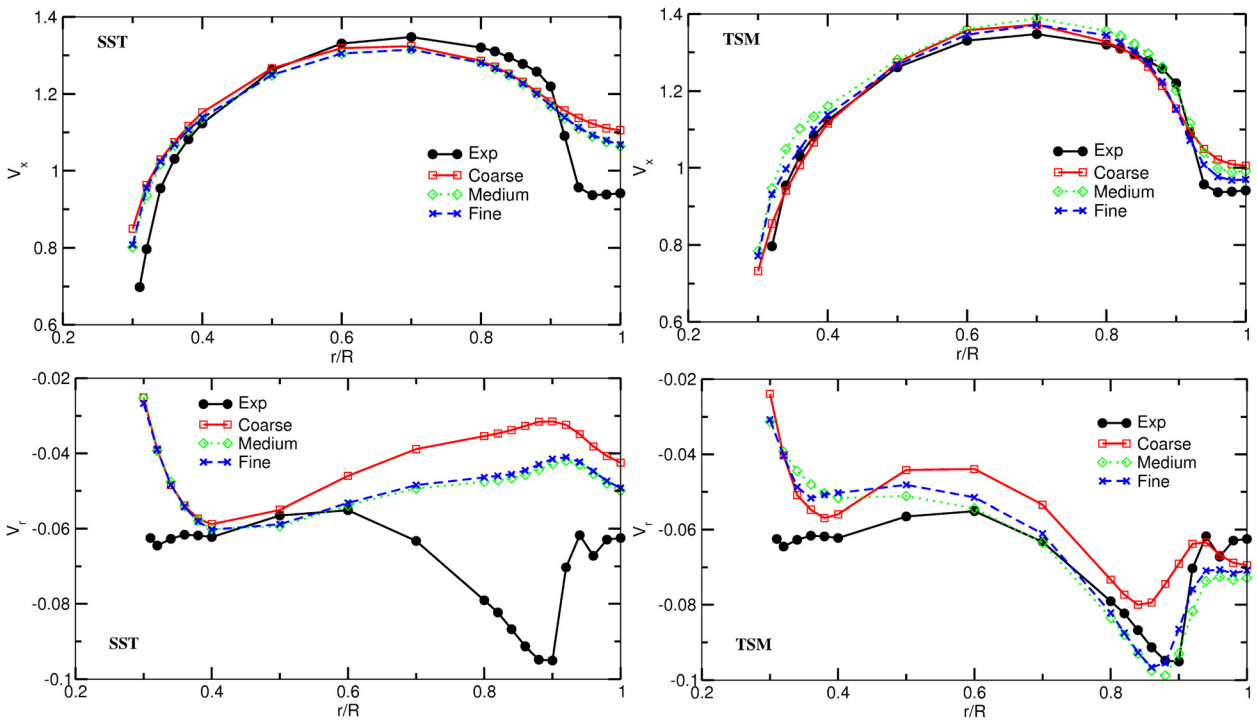

Fig. 3 Circumferential-averaged axial (top) and radial (bottom) velocity for grid resolution study

incorporation of a viscous wall destruction term in the k_T and k_L equations. Detailed explanations can be found in Ref. [10].

In addition to simulations of the advance ratios corresponding to the four cases ($J = 0.98$, 1.1, 1.27, 1.51) measured in the water-tunnel test, simulations were also conducted at $J = 0.5$ and 1.6 to investigate the behavior of the turbulence models under off-design conditions, particularly at the higher-load condition, i.e., lower advance ratio ($J = 0.5$). Simulation at the higher-load condition was considered particularly important because it is known that fully turbulent RANS simulation results have observed increasing discrepancy with increasing propeller load as compared to model scale experiments, because of the inappropriate assumption that the flow around the propeller is fully turbulent whether in model scale or in full scale. This tendency prevents most RANS CFD simulations [40–43] from quantitatively predicting viscous flow aspects of propeller blade flows, and hence the test case of $J = 0.5$ is expected to be a challenging one for the turbulence models in the RANS solver.

The flow solver uses a cell centered finite volume method for three-dimensional generalized grids. Implicit first order Euler time stepping typically used in steady-state simulations was employed because only steady solutions are desired in this study. The code is implemented using second-order spatial accuracy in both convective and diffusive terms, and Roe's flux difference splitting scheme is used for reconstruction of convective face fluxes. One Newton iteration was performed for each time step, and five Gauss-Seidel iterations were used when solving the linear system. The turbulent equations are decoupled from the mean flow solver, and communication of variables between turbulent and mean flow occurs after each time step. Steady state simulations with local time stepping were conducted in a relative rotating frame with a constant rotational speed corresponding to each test condition. An inflow/outflow characteristic based boundary condition was applied to the outer boundary, where a constant rotational speed was specified in the opposite direction as observed in the relative rotating frame. Uniform flow was assumed as the initial condition. Fully turbulent simulations were able to be initiated from uniform flows for all test cases, and this is also true for turbulent transition simulations at lower load conditions, for $J > 0.5$. The only case facing numerical difficulty was the turbulent transition simulation at the highest load $J = 0.5$. For this case, it was necessary to run laminar flow first, and then start the turbulent transition simulation using the converged laminar flow solution as the initial condition (after 10,000 iterations). Because there was some small unsteadiness in this complex flow, it was not possible to drive the residuals to machine zero, although they were typically reduced at least six orders of magnitude versus their initial values. Instead, the behavior of integrated properties, such as the propeller total thrust shown in Fig. 4, was used to determine when the solution had converged. Once the fluctuation in total thrust was less than 0.5 N, results were considered to be converged.

4.2 Propeller Performance Prediction. For all of the calculated results, both the pressure and viscous shear stresses were integrated over all of the blade and shaft surfaces, and the total force and moment vectors were resolved into the three coordinate directions (x, y, z). The axial force (thrust T) and moment around the propeller axis (torque Q) define the thrust and torque coefficients, K_T and K_Q, respectively. The predicted overall thrust and torque are presented in Fig. 5 along with experimental measurements performed in the CDNSWC water tunnel and towing basin. In the water-tunnel test by Chesnakas and Jessup [1], the velocity measurements were performed at four advance ratios of $J = 0.98$, 1.1, 1.27, and 1.51. In the fully turbulent simulations, underestimations in thrust and over-predictions in torque were observed, and prediction accuracy deteriorated with increased propeller load, i.e., reduced advance ratio. For the case of $J = 0.5$, the over-prediction in torque is 19% and the underprediction in thrust is 15%. Simulation cases at lower advance ratio have lower

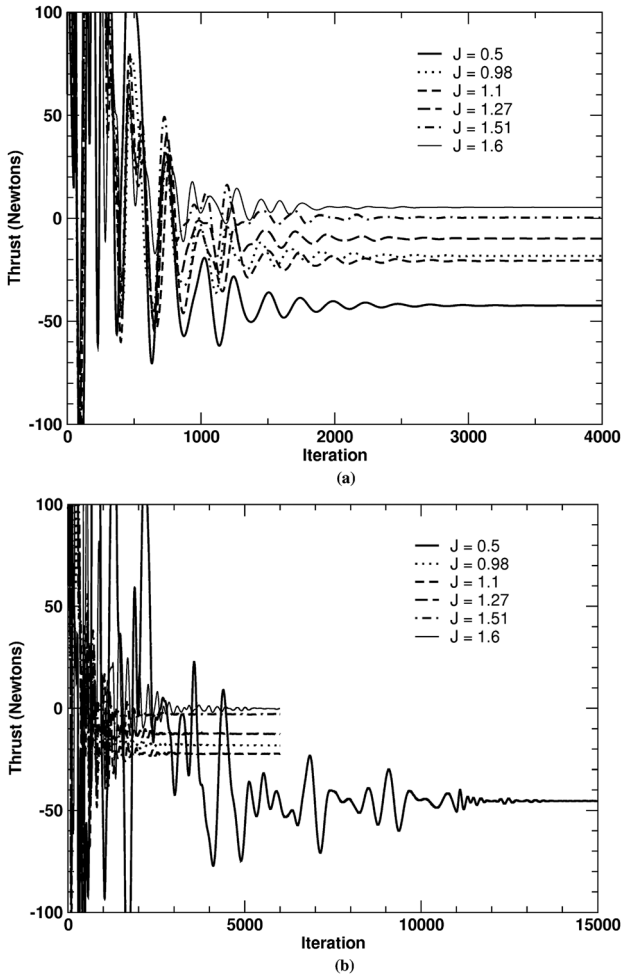

Fig. 4 Convergence history of total thrust: (*a*) SST simulations, and (*b*) TSM simulations

Reynolds numbers and are therefore likely to have larger laminar flow regions and delayed turbulent transition. Rhee and Joshi [3] performed laminar and fully turbulent simulations with the k-ω turbulence model on this propeller and discovered that the pressure component force is dominant in determining K_T, whereas K_Q

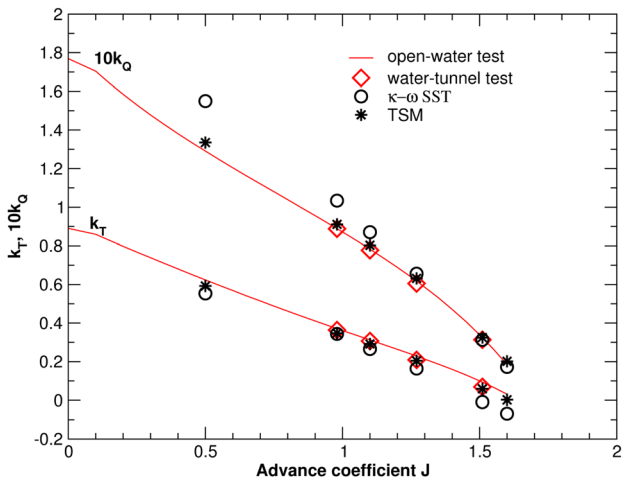

Fig. 5 Comparison of measured and computed propeller characteristics

is more dependent on the frictional component and sensitive to the viscous stresses exerted on the propeller blades. This helps to explain the larger error in computed K_Q at $J=0.5$, and suggests that the fully turbulent simulation is not adequate for propeller flows at high load when laminar and/or transitional boundary layers are prevalent.

Once boundary-layer transition was considered in the simulations, the computed thrust and torque coefficients showed various levels of improvement for all of the test cases. The agreement in K_T at near design conditions, for $J=0.98$, 1.1, and 1.27, was very good with relative errors less than 5%. Improvement in the torque predictions were also quite good and relative differences were found to be between 2.5–4.4% for cases of $J<1.6$, and 9% for $J=1.6$. The turbulent transition simulation showed considerable advantage in performance prediction at the highest-load condition, $J=0.5$, where the agreement in predicted thrust and torque indicated a difference of 5.1% and 3.4% compared to measured values. In contrast, the fully turbulent SST k-ω simulations predicted differences of 15% and 19% in thrust and torque, respectively. The results suggest that consideration of boundary-layer transition is a key component of accurate CFD simulations at higher-load conditions. At lower load conditions, torque predictions were also in better agreement in transition simulations, within 3.8% at $J=1.51$ and 9.0% at $J=1.6$. Because of the fact that thrust is near zero when $J=1.51$ and 1.6, calculated thrust with the TSM model showed improvement compared to SST model, but the relative errors remain large when compared to measured values. Absolute errors in K_T, however, were reduced from 0.099 with the SST k-ω model to 0.028 with the transition-sensitive model.

4.3 Velocity Predictions in the Wake Region. Accurate wake flow simulation plays an important role in design and performance analysis of a marine propulsion system. The tip-vortex cavitation in the wake is closely associated with noise generation, ship vibrations, and efficiency decay. This section attempts to highlight the capability of different modeling approaches for predicting wake flow details related to viscous effects. For comparison, detailed velocity measurements behind the propeller made in the water-tunnel test are available for $J=1.1$ at a downstream location $x/R=0.2386$, measured from the propeller mid plane. The measurements were made to examine the behavior of the tip-vortex flow. The measurements included 1024 circumferential positions and 49 radial positions. In the radial direction, the region of tip vortex had fine resolution with 10^{-4} m spacing and the middle span had a measurement spacing of 10^{-2} m.

Figure 6 presents contours of the relative velocity components in the axial, radial and tangential directions. All values are observed in the rotating frame and normalized by the tunnel velocity U_∞. Fig. 7 provides a close-up view of the axial velocity contours in the region of the tip vortex. Observing Figs. 6 and 7, the water-tunnel test showed regions of minimum and maximum axial velocity in the vicinity of tip radius at 0.93 R and 0.90 R, respectively. This is the result of the strong rotational flow within the tip vortex. The location of the local minimum axial velocity near the propeller tip radius reflects the accuracy of the predicted tip-vortex location, which is important for obtaining good thrust prediction. The TSM simulations successfully captured the minimum and maximum axial velocities at similar locations as the experiments, with a local minimum axial velocity at 0.96 R, and a maximum value at 0.88 R.

Figure 8 shows the circumferentially averaged velocity components along the radial span at a downstream plane at $x/R=0.2386$ for $J=1.1$. Both the fully turbulent and transition-sensitive simulations are able to capture the mid span flow acceleration as indicated by the local maximum in axial velocity. The TSM simulation shows better agreement with water-tunnel velocity measurements in the tip region because of better resolution of the tip-vortex flow in that region. This is also reflected in the improvement in thrust and torque predictions by the TSM simulations as

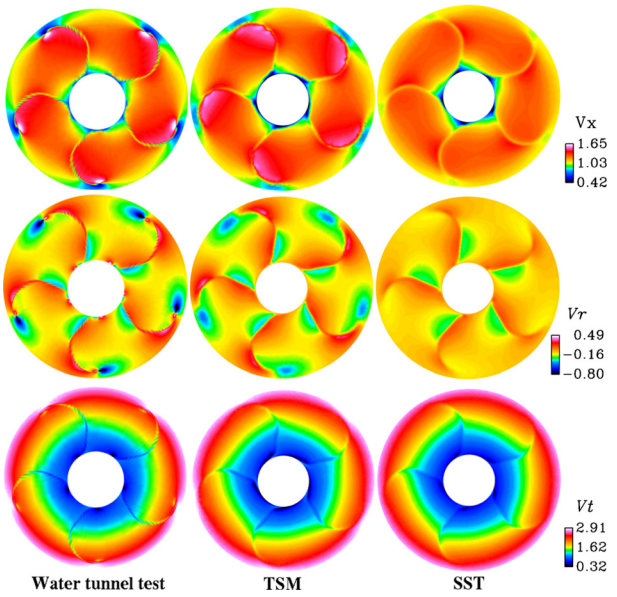

Fig. 6 Relative velocity components (axial velocity V_x, radial velocity V_r, and tangential velocity V_t) downstream of the propeller at $x/R=$ 0.2386 for $J=1.1$

shown in Fig. 5. The negative radial velocity V_r indicates flow contraction because of the acceleration of the fluid by the propeller, and is dependent upon the thrust exerted by the propeller. The greater the thrust produced by the propeller for a given speed, the stronger the contraction will be. In the upper span, especially near the tip region, the TSM simulation is able to quantitatively capture the flow contraction as observed in the water-tunnel test, whereas the fully turbulent simulation misses the strong contraction in the upper span and tip region, helping to explain the underestimated thrust by the fully turbulent simulations. In the region near the hub, the predicted radial velocities by both turbulence models showed poor agreement with the water-tunnel measurements. This problem was also reported by Rhee and Joshi [3] and was suspected to be caused by the unsatisfactory boundary-layer development near the hub, and insufficient mesh resolution in that area. After a close inspection of the water-tunnel test data, it is noticed that flow contractions occur in a large region (from hub to 0.7 R) on the pressure side, but also in a small region on the suction side (from hub to 0.35 R) with similar strength (local extreme value $V_r\approx-0.35$). In the current study, the large contraction region on the pressure side is captured accurately, whereas the small

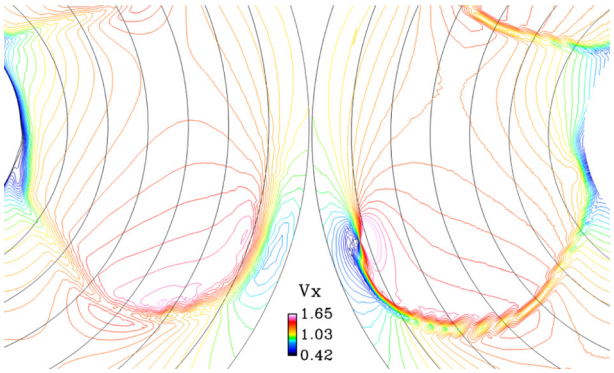

Fig. 7 Comparison between water-tunnel test (right) and TSM solution (left) of the tip-vortex region, axial velocity at $x/R=$ 0.2386 for $J=1.1$ (black curves denote radial locations from 0.4 R to 1.0 R)

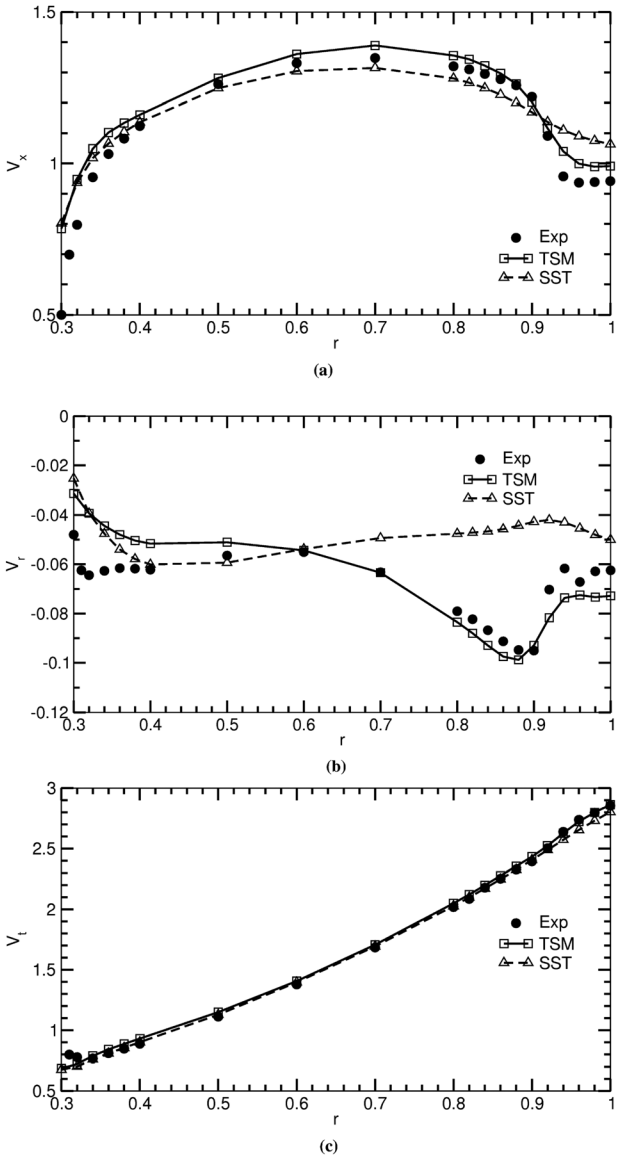

Fig. 8 Circumferentially averaged velocity components on $x/R = 0.2386$ plane for $J = 1.1$: (*a*) axial velocity V_x, (*b*) radial velocity V_r, and (*c*) tangential velocity V_t

contraction region close to the hub on the suction side is missed, even with increased overall grid resolution in the fine grid. Further refinement of the hub surface mesh and refinement of volume grid along the blade wake paths might be required to tackle this problem.

The predicted tip-vortex flow still indicates excessive dissipation, as shown in both axial and radial velocities, which may be because of the fact that the model does not include any modifications for the strongly rotating flow that occurs within the vortex, a common weakness of most eddy-viscosity models. It is possible that results could be further improved by implementing a transition-sensitive version of a nonlinear k-ε or k-ω model that is sensitized to the effects of rotation on turbulent flow; for example the model of Vlahostergios et al. [44]. The fully turbulent simulations showed very weak and smaller size of the tip-vortex flow, and the negative radial velocities near the tip region observed in the water-tunnel test and turbulent transition simulations were completely missed. Overall, the transition-sensitive model showed significantly better agreement in both axial and radial velocity distribution, although the tangential component by both simulations showed a very similar pattern and good agreement with test data.

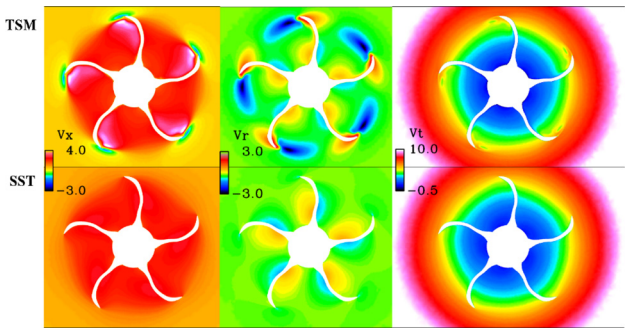

Fig. 9 Relative velocity components (axial velocity V_x, radial velocity V_r, and tangential velocity V_t) at propeller cross section at $x/R = 0.05$ for $J = 0.5$: TSM (top) and SST (bottom)

4.4 Flow Features at High Load, $J = 0.5$. RANS CFD simulations commonly experience lower accuracy in predictions of thrust and torque at higher propeller loads and large errors occur even at $J = 0.9$ for P5168 [3]. To the authors' knowledge, RANS simulations at high load ($J = 0.5$) for this propeller have not been reported in the open literature. Because any advantage of a turbulent transition model in better capturing the tip-vortex flow should be most obvious under high load, this section pays particular attention to the results for that case. Because no experimental data for the velocity field is available at this load condition, only the CFD solutions are shown in Fig. 9, which compares the relative velocity components on a cutting plane across the propeller at $x/R = 0.05$. The fully turbulent simulation shows similar flow characteristics with the turbulent transition solution in the area that lies below the middle span. However the large velocity gradients in the tip region shown in all three of the velocity components are resolved only in the TSM solutions.

To further investigate the development of tip-vortex flow, contours of axial velocity along the blade tip are plotted at several locations between the leading edge and trailing edge in Fig. 10, where surface flow streamlines and pressure coefficient C_p on propeller surfaces are also presented. Figure 10(*a*) visualizes only the negative axial flow regions near the blade edge in the TSM solutions and Fig. 10(*b*) highlights the edge regions where the axial velocity $V_x \leq 1.0$ in the k-ω SST solutions. Figures 10(*c*) and 10(*d*) samples the axial velocities and pressure coefficients at the center of the vortex flows at each cross section. The tip-vortex flows resolved by the TSM and SST models show substantial differences. In the transition-sensitive solutions, negative axial velocities are found in the vicinity of the tip radius all the way from leading edge to trailing edge and the largest value of $-C_p$ appears at the mid plane $x/R = 0$, where the vortex core pressure also shows a corresponding jump. However, in the fully turbulent simulations, a near zero negative axial velocity is observed at only one sample section at the leading edge, behind which axial flows near the tip region are all positive. In the turbulent transition solution, the surface flow streamlines merge near the leading edge, indicating the flow lifting from the surface and rolling up into a vortex core. The low pressure near the leading edge on the suction side, where a strong suction side tip vortex occurs, is clearly resolved in the turbulent transition simulation. Comparing the two solutions shown in Fig. 10, the simulation with the TSM model generates lower pressure in a narrow region near the leading edge and tip radius, and higher pressure in a large area at lower radii and the trailing edge.

Looking at the limiting streamlines on the pressure surface in Fig. 11, the transition flow patterns are also complicated because of the presence of laminar separation and turbulent reattachment regions. For the transition simulation in Fig. 11(*a*), streamlines originating from the leading edge are parallel to the tangential

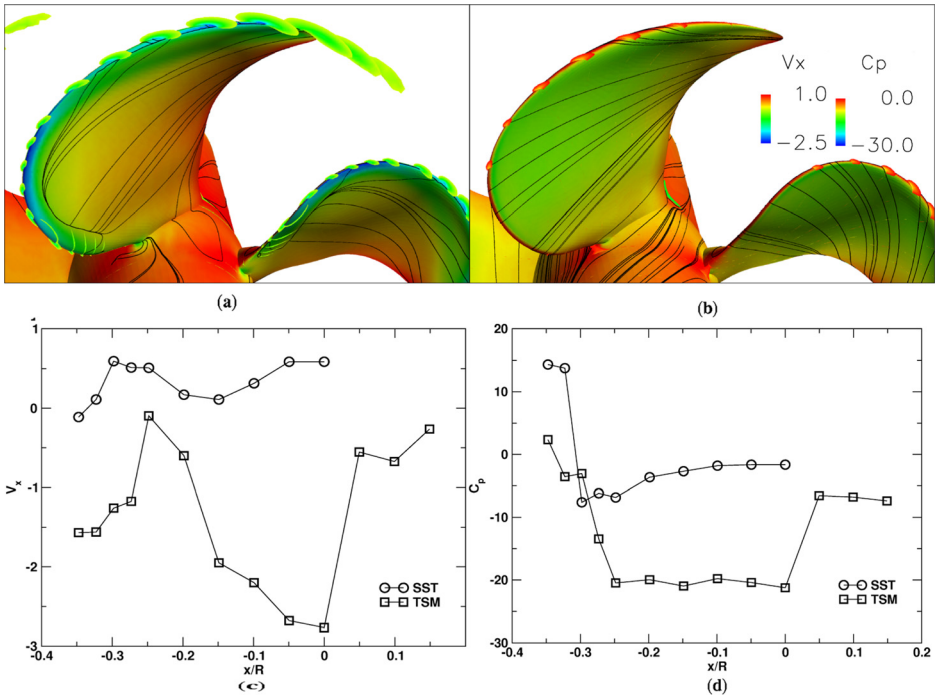

Fig. 10 Tip-vortex strength at high-load condition, $J = 0.5$, propeller surfaces are colored by pressure coefficient and show surface streamlines: (*a*) tip region axial velocity contours by TSM, (*b*) tip region axial velocity contours by SST, (*c*) axial velocity in the tip vortex, and (*d*) pressure coefficient in the tip vortex

direction indicating well-defined leading-edge attached flows. As the streamlines approaching trailing edge, they become more radially oriented and end at the blade tip. This tendency is more significant for the lower span region, where streamlines are converged near the trailing edge where separation occurs. A circular cutting plane intersecting with the converged streamlines near the trailing edge is extracted in Fig. 12 to inspect flow details in that region. The velocity vectors show that a thin layer of separation occurs behind the converged streamlines and turbulent kinetic energy starts to increase because of separation induced transition. In contrast, streamlines in the fully turbulent simulation, as shown in Fig. 11(*b*), are nearly parallel running from leading edge to trailing edge. Boundary-layer turbulence is much stronger in the fully turbulent simulation and turbulence increases immediately from the blade leading edge at all blade span locations.

Accurate prediction of the wall shear stress distribution on the propeller blade is important for analyzing the flow characteristics of a propeller design. When transition takes place on blade surfaces, the viscous shear stress is expected to be significantly different from a fully turbulent flow simulation. Figure 13 presents the shear stress contours on the blade surfaces for both models. The suction side distribution predicted in the transition simulation (Fig. 13(*a*)) shows a strong shear stress gradient along the radial direction, where the lower span regions close to the hub (approximately $<0.4\ R$) are mainly occupied by laminar flow, indicated by the lower values of shear stress. Turbulent flow is observed in the upper span near the blade tip. The transition line from laminar to turbulent flow is aligned with a radius section near $0.4R$ identified by a sudden increase of the shear stress value. The fully turbulent calculation presents a different pattern (Fig. 13(*b*)) on the suction side with a negative shear stress gradient pointing approximately from leading edge to trailing edge, i.e., the shear stress varies primarily along the tangential direction.

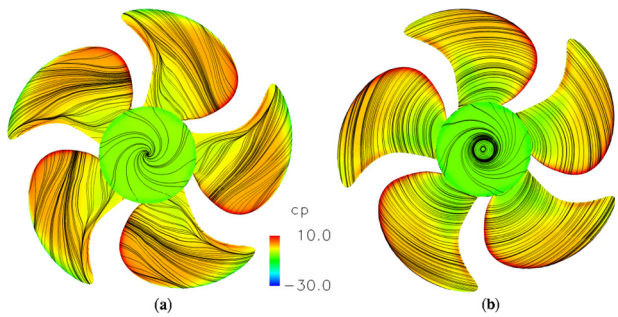

Fig. 11 Pressure distribution and limiting streamlines on pressure side for $J = 0.5$: (*a*) TSM, and (*b*) SST

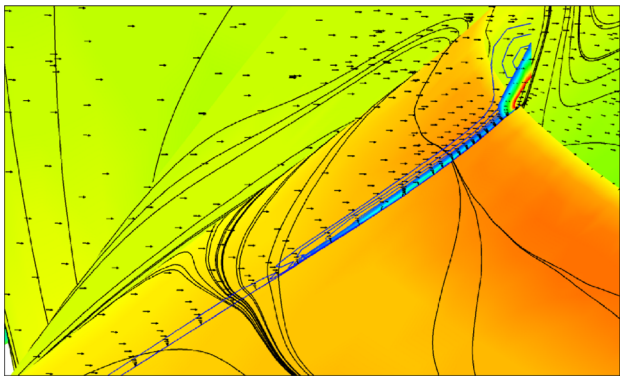

Fig. 12 Velocity vectors and turbulent kinetic energy on a circular cutting plane across the converged blade limiting streamlines on pressure side for transition case at $J = 0.5$

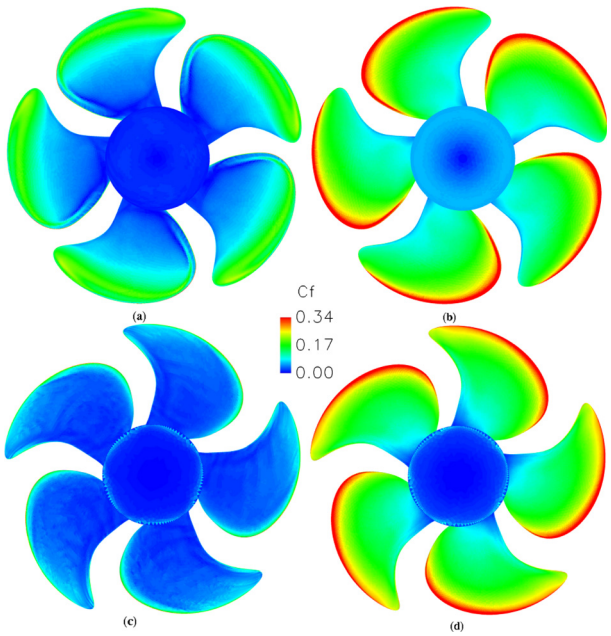

Fig. 13 Skin fraction distribution on propeller surfaces for *J* = *0.5*: (*a*) suction side by TSM, (*b*) suction side by SST, (*c*) pressure side by TSM, and (*d*) pressure side by SST

Shear stress on the pressure sides showed similar distributions in the TSM and SST calculations, but with different levels of the absolute stress. This result suggests that the flow was predicted to be laminar over almost the entire pressure surface using the TSM model; in contrast with the fully turbulent prediction using the SST model.

An interesting observation in the transition simulation is the strong spanwise gradient of shear stress on suction surfaces. It is expected that this flow behavior is primarily related to the presence of laminar and turbulent flow regions. To confirm this, contours of turbulent kinetic energy were extracted, as shown in Fig. 14, at various span locations ranging from 0.4 R to 0.9 R, to inspect the turbulent boundary-layer development in those areas. It is noticed that laminar separations occur in the area where a sudden increase of shear stress appears at the blade leading edge between 0.5 R–0.7 R followed by reattachment of the boundary layer. Moving from lower span to upper span, the size of the separation bubbles and the origination of boundary-layer turbulence increase concurrently. At higher span, above 0.8 R approximately,

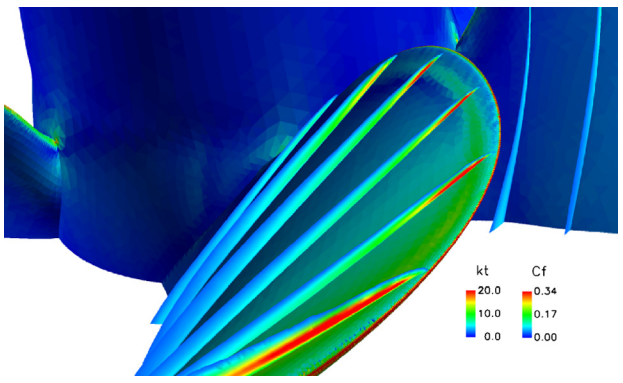

Fig. 14 Turbulent kinetic energy at various spans (*r/R* = [0.4–0.9]) on suction surface in transition case (blade surface is colored by skin fraction coefficient C_f)

relative velocity and shear stress are much higher and the flow is fully turbulent from the leading edge to trailing edge.

5 Summary and Conclusions

Simulations for incompressible flow around marine propeller 5168 were conducted using a transition-sensitive k-ω eddy-viscosity turbulence model implemented into the Loci-CHEM flow solver. Simulations using an eddy-viscosity model that is only capable of predicting fully turbulent boundary-layer flow (k-ω SST) were also performed for comparison. Results were compared with experimental measurements under various flow conditions, including design and off-design conditions. The objectives were to demonstrate the capability of a transition-sensitive turbulence model for 3D turbulent flows around complex geometries, to determine the relative importance of resolving boundary-layer transitional effects in this class of flow, and to document a potentially effective method to handle the turbulent transition that usually occurs under high load on the propeller blade surface, in order to improve prediction accuracy of propeller performance.

The marine propeller 5168 has a design advance ratio of $J = 1.27$. Computations were performed at various advance ratios from 0.5 to 1.6, which covered both high- and low-load conditions. With the transition-sensitive model, prediction accuracy in propeller performance improved to varying degrees depending on the load condition. At near design conditions, $J = 0.98$, 1.1, and 1.27, predicted torque and thrust coefficients are within 5% and 4.4% of measured values. The most significant advantage of the transition-sensitive model was apparent in the computation at low advance ratio, $J = 0.5$, where the relative differences were 5.1% and 3.4% in thrust and torque prediction, respectively. By contrast, existing CFD results by fully turbulent simulations experienced a large discrepancy with increasing propeller load, even at $J = 0.98$. To the authors' knowledge based on the open literature, this work is the first attempt of RANS calculation for P5168 at high-load condition $J = 0.5$.

In addition to the global quantities, boundary-layer flow over the propeller blades, the associated tip vortex, and flow separation behavior were analyzed and discussed in some detail. Compared to the fully turbulent flow simulations, the transition-sensitive turbulence model was able to better resolve the strength of the tip vortices. Surface flow streamlines obtained by the transition-sensitive computations also resolved blade-surface flow separations. The application of the transition-sensitive turbulence model in the propeller flows will likely not only benefit the prediction of blade-surface flows and corresponding force and moment calculations, but also provide more correct originations of tip-vortex flows and lead to improved calculations for wake flows. This is evidenced by the predicted velocity profiles at a downstream location in the wake region. The transition-sensitive simulations obtained similar flow patterns compared to the water-tunnel measurements and the fully turbulent simulations showed excessive dissipation for the tip-vortex flows.

Results obtained in this effort are promising in high-load marine-propeller simulations and the investigated transition-sensitive turbulence model is practical and effective for 3D flows over complex geometries. Future work will investigate the ability of the models to predict the downstream development of the wake paths, and to investigate other modifications to the turbulence model (i.e. inclusion of rotation/curvature effects) that may further improve overall predictive performance.

Nomenclature

C = propeller chord length
C_p = pressure coefficient, $(p - p_\infty)/(\frac{1}{2}\rho U_\infty^2)$
C_f = skin fraction coefficient, $\tau_w/(\frac{1}{2}\rho U_\infty^2)$
D = propeller diameter, 0.4027 m
J = advance coefficient, $U_\infty/(nD)$
k_L = laminar kinetic energy
K_Q = torque coefficient, $Q/(\rho n^2 D^5)$

k_T = turbulent kinetic energy
K_T = thrust coefficient, $Q/(\rho n^2 D^4)$
n = propeller rotational speed, rev/s
p = static pressure
p_∞ = freestream static pressure
q = root-mean-square (rms) fluctuation of velocity, $q = \sqrt{2k_T}$
Q = torque
R = propeller radius
Re = Reynolds number based on free stream and propeller diameter
Re_b = blade Reynolds number, evaluated at $r = 0.7R$, $\left[U_\infty^2 + (2\pi rn)^2\right]^{1/2} \cdot C/\upsilon$
T = thrust
Tu_∞ = free stream turbulence intensity
U_∞ = inflow velocity in the stationary frame
V_x = axial velocity, normalized by U_∞
V_r = radial velocity, normalized by U_∞
V_t = tangential velocity in the rotating frame, normalized by U_∞
x = axial coordinate, from propeller mid plane
ρ = densityρ
ν = kinematic viscosity

References

[1] Chesnakas, C. J., and Jessup, S. D., 1989, "Cavitation and 3-D LDV Tip-Flowfield Measurements of Propeller 5168," CRDKNSWD/HD-1460-02, Carderock Division, Naval Surface Warfare Center.
[2] Paterson, E. G., Wilson, R. V., and Stern F., 2003, "General-Purpose Parallel Unsteady RANS Ship Hydrodynamics Code: CFDSHIP-IOWA IIHR," Technical Report No. 432.
[3] Rhee, S. H., and Joshi, S., 2005, "Computational Validation for Flow around a Marine Propeller Using Unstructured Mesh Based Navier-Stokes Solver," JSME Int. J., Ser. B, **48**(3), pp. 562–570.
[4] Hsiao, C., and Chahine, G. L., 2008, "Scaling of Tip Vortex Cavitation Inception for a Marine Open Propeller," 27th Symposium on Naval Hydrodynamics, Seoul, Korea.
[5] Hsiao, C., and Pauley, L. L., 1999, "Numerical Computation of Tip Vortex Flow Generated by a Marine Propeller," ASME J. Fluids Eng., **212**, pp. 638–645.
[6] Oh, K.-J., and Kang, S.-H., 1995, "Numerical Calculation of the Viscous Flow around a Propeller Shaft Configuration," Int. J. Numer. Methods Fluids, **21**(1), pp. 1–13.
[7] Stanier, M., 1998, "The Application of RANS Code to Investigate Propeller Scale Effects," Proceeding of the 22nd Symposium on Naval Hydrodynamics, Washington, D.C., pp. 222–233.
[8] Chen, B., and Stern, F., 1999, "Computational Fluid Dynamics of Four-Quadrant Marine-Propulsor Flow," J. Ship Res., **43**(4), pp. 218–228.
[9] Funeno, I., 2002, "On Viscous Flow around Marine Propellers-Hub Vortex and Scale Effect," J. Kansai Soc. Nav. Archit., **2002**(238), pp. 17–27.
[10] Walters, D. K., and Cokljat, D., 2008, "A Three-Equation Eddy-Viscosity Model for Reynolds-Averaged Navier-Stokes Simulations of Transitional Flow," ASME Trans. J. Fluids Eng., **130**(12), pp. 121401.1–121401.14.
[11] Luke, E., 2007, "On Robust and Accurate Arbitrary Polytope CFD Solvers (Invited)," 18th AIAA Computational Fluid Dynamics Conference, Miami, FL, AIAA 2007-3956.
[12] Luke, E., and Cinnella, P., 2007, "Numerical Simulations of Mixtures of Fluids Using Upwind Algorithms," Comput. Fluids, **36**(10), pp. 1547–1566.
[13] Tong, X.-L., and Luke, E., 2004, "Turbulence Models and Heat Transfer in Nozzle Flows," AIAA J., **42**(11), pp. 2391–2393.
[14] Wu, J., Tang, L., Luke, E., Tong, X.-L., and Cinnella, P., 2002, "Comprehensive Numerical Study of Jet-Flow Impingement over Flat Plates," J. Spacecr. Rockets, **35**(1), pp. 357–366.
[15] Liu, Q., Luke, E., and Cinnella, P., 2005, "Coupling Heat Transfer and Fluid Flow Solvers for Multi-Disciplinary Simulations," J. Thermophys. Heat Transfer, **19**(4), pp. 417–427.
[16] Tong, X.-L., and Luke, E., 2005, "Eulerian Simulations of Icing Collection Efficiency Using a Singularity Diffusion Model," 43rd AIAA Aerospace Sciences Meeting and Exhibit, Reno, NV, AIAA Paper 2005-01246.
[17] Kalitzin, G., Wu, X., and Durbin, P. A., 2003, "DNS of Fully Turbulent Flow in a LPT Passage," Int. J. Heat Fluid Flow, **24**, pp. 636–644.
[18] van Driest, E. R., and Blumer, C. B., 1963, "Boundary Layer Transition, Free Stream Turbulence, and Pressure Gradient Effects," AIAA J., **1**(6), pp. 1303–1306.
[19] Abu-Ghannam, B. J., and Shaw, R., 1980, "Natural Transition of Boundary Layers-The Effects of Turbulence, Pressure Gradient, and Flow History," J. Mech. Eng. Sci., **22**, pp. 213–228.
[20] Mayle, R. E., 1991, "The Role of Laminar-Turbulent Transition in Gas Turbine Engines," ASME J. Turbomach., **113**, pp. 509–537.
[21] Fasihfar, A., and Johnson, M. W., 1992, "An Improved Boundary Layer Transition Correlation," ASME Paper No. 92-GT-245.
[22] Praisner, T. J., and Clark, J. P., 2007, "Predicting Transition in Turbomachinery-Part I: A Review and New Model Development," ASME J. Turbomach., **129**, pp. 1–13.
[23] Edwards, J. R., Roy, C. J., Blottner, F. G., and Hassan, H. G., 2001, "Development of a One-Equation Transition/Turbulence Model," AIAA J., **39**, pp. 1691–1698.
[24] Wang, C., and Perot, B., 2002, "Prediction of Turbulent Transition in Boundary Layers Using the Turbulent Potential Model," J. Turbul., **3**, pp. 22–36.
[25] Walters, D. K., and Leylek, J. H., 2004, "A New Model for Boundary Layer Transition Using a Single-Point RANS Approach," ASME J. Turbomach., **126**, pp. 193–202.
[26] Suzen, Y. B., and Huang, P. G., 2000, "Modeling of Flow Transition Using an Intermittency Transport Equation," ASME Trans. J. Fluids Eng., **122**, pp. 273–284.
[27] Steelant, J., and Dick, E., 2001, "Modeling of Laminar-Turbulent Transition for High Freestream Turbulence," ASME Trans. J. Fluids Eng., **123**, pp. 22–30.
[28] Menter, F. R., Langtry, R. B., Likki, S. R., Suzen, Y. B., Huang, P. G., and Volker, S., 2006, "A Correlation-Based Transition Model Using Local Variables-Part I: Model Formulation," ASME J. Turbomach., **128**, pp. 413–422.
[29] User Guide Fluent 6.12, Ansys Inc., Canonsburg, PA.
[30] Mayle, R. E., and Schulz, A., 1997, "The Path to Predicting Bypass Transition," ASME J. Turbomach., **119**, pp. 405–411.
[31] Coupland, J., 1990, ERCOFTAC Special Interest Group on Laminar to Turbulent Transition and Retransition, T3A and T3B Test Cases.
[32] Luke, E. A., and George, T., 2005, "Loci: A Rule-Based Framework for Parallel Multidisciplinary Simulation Synthesis," J. Funct. Program., **15**(3), pp. 477–592.
[33] Luke, E. A., Tong, X.-L., and Cinnella, P., 2006, "Numerical Simulations of Fluids with a General Equation of State," 44th Aerospace Sciences Meeting, Reno, NV, AIAA 2006-12951.
[34] Menter, F. R., 1992, "Improved Two-Equation K-omega Turbulence Models for Aerodynamic Flows," Ames Research Center, Moffett Field, NASA Technical Memorandum, 103975.
[35] Gaither, J. A., Marcum, D. L., and Mitchell, B., 2000, "SolidMesh: A Solid Modeling Approach to Unstructured Grid Generation," 7th International Conference on Numerical Grid Generation in Computational Field Simulations, Whistler, BC.
[36] Marcum, D. L., 2001, "Efficient Generation of High Quality Unstructured Surface and Volume Grids," Eng. Comput., **17**(3), pp. 211–233.
[37] Marcum, D. L., and Gaither, J. A., 1999, "Mixed Element Type Unstructured Grid Generation for Viscous Flow," 14th AIAA Computational Fluid Dynamics Conference, Norfolk, VA, AIAA Paper 99-3252.
[38] Remotigue, M. G., 1999, "Structured Grid Technology to Enable Flow Simulation in an Integrated System Environment," Ph.D. dissertation, Mississippi State University, MS.
[39] Menter, F. R., 1994, "Two-Equation Eddy-Viscosity Turbulence Models for Engineering Applications," AIAA J., **32**(8), pp. 1598–1605.
[40] Ito, M., 1987, "Calculation of Viscous Effects on Propeller Open Characteristics," Trans. West-Japan Soc. Nav. Archit., **73**, pp. 83–96.
[41] Uto, S., 1992, "Computation of Incompressible Viscous Flow around a Marine Propeller," Jpn. Soc. Nav. Archit. Ocean Eng., **172**, pp. 213–224.
[42] Uto, S., 1993, "Computation of Incompressible Viscous Flow around a Marine Propeller, 2nd Report: Turbulent Flow Simulation," Jpn. Soc. Nav. Archit. Ocean Eng., **173**, pp. 67–75.
[43] Uto, S., 1994, "Basic Study on the Scale Effect of the Viscous Flow around a Marine Propeller," J. Kansai Soc. Nav. Archit., **222**, pp. 33–39.
[44] Vlahostergios, Z., Yakinthos, K., and Goulas, A., 2009, "Separation-Induced Boundary Layer Transition: Modeling with a Non-linear Eddy-Viscosity Model Coupled with the Laminar Kinetic Energy Equation," Int. J. Heat Fluid Flow, **30**(4), pp. 617–636.